

Planetary Orbits Around Binary Star Systems

A. A. Lascelles
School of Physics and Astronomy
University of Southampton
SO17 1BJ
United Kingdom
E-mail: aal1g13@soton.ac.uk

May 3, 2016

Abstract

A simulation of planetary orbits around a binary star system using a Runge-Kutta procedure is presented. Through choices of initial velocities and positions, orbit stability is tested for a range of P- and S-type orbits confined to a disc in the x - y plane around the central stars. The boundary conditions and time-evolution of such orbits is explored. Chaos theory, habitable zones, and other such related phenomena are discussed.

1 Introduction

Binary stars are systems containing two companion stars orbiting each other via gravitational attraction with a common centre of mass. It is generally believed that more than half of all star systems we observe contain multiple stars[1]. The search for a habitable exoplanet is currently an active area of research in astronomy, and recent results confirm the existence of exoplanets that orbit binary star systems[2]. Studying such planets is of great importance for exo-biology. For life to exist, the planet on which it lives must keep to a stable orbit over long time-scales. This is needed because the time for protoplanetary formation and for evolution would encompass billions of orbital periods.

There are two species of orbit possible for a planet in a binary system, namely P-type and S-type. P-type orbits will orbit the combined centre of mass of the two stars as if they are one single body whereas planets in an S-type orbit only travel around one of the stars with the other acting as a perturbation[3].

To solve the differential equations involved in a 3-body system, the equations of motion must first be derived (as shown in appendix A). This assumes Newtonian physics is appropriate, and combines Newton's 2nd law with the gravitational attraction of the two stars. Satellites do not strictly follow this motion because of perturbations from other planets, comets, asteroids, and even effects such as accretion changing the gravitational field. However, for the scope of this paper, where we neglect such effects, they can be considered valid. Throughout, we assume that masses are in units of solar masses (M_{\odot}) so that $M = 1M_{\odot}$, distances are in terms of astronomical units (AU) so that $R = 1AU$, and time in units of years. It is further assumed that the system is confined to a 2D plane, as we observe in most solar systems.

In the following section, the methodology of this paper will be discussed. The two-fold method includes mathematical manipulation of differential equations, derived in appendix A, in order to achieve a form that can be computationally evaluated. The purpose of Section 3, which forms the main bulk of the scientific findings, is to explain the physics behind the various orbits found. Boundary conditions for each type of orbit will be discussed along with the reasons behind the shape of the S-type, P-type, circular, and elliptical orbits found together with the extension detailing chaotic orbits and habitable zones. Section 4 concludes the findings of this paper, whilst the appendix is where derivations of the equations of motion used herein can be found.

2 Methodology

2.1 Manipulation of Differential Equations

In order to make the differential equations suitable for the computational Runge-Kutta algorithm, they are first non-dimensionalised and then converted into four first-order equations. These four equations can be sub-divided into two representing the x -velocity and x -acceleration and two representing the y -velocity and y -acceleration as detailed in the following paragraphs.

First consider a pair of stars obeying Kepler's laws of motion and rotating with a period T around their common centre of mass on a circle of radius R . Their Cartesian coordinates will be given by,

$$X_1 = R \cos(\Omega t), \quad Y_1 = R \sin(\Omega t), \quad (1)$$

$$X_2 = -R \cos(\Omega t), \quad Y_2 = -R \sin(\Omega t). \quad (2)$$

Introducing a planet of negligible mass into this scenario creates the 3-body system where the position, $r_{1,2}$, of the planet from star 1 or star 2 is given by,

$$r_{1,2}^2 = (x - X_{1,2})^2 + (y - Y_{1,2})^2. \quad (3)$$

Here, R is the radial distance coordinate, where the stars are set apart at a distance R , $r_{1,2}$ are the radial distances of the planet from star 1 and 2 respectively, $X_{1,2}$ and $Y_{1,2}$ are the distances from the origin of star 1 and 2 respectively, x and y are the positions of the planet with respect to the origin, and angular frequency $\Omega = \frac{2\pi}{T}$ is the inverse of the period of orbit, T , for the two stars.

This allows us to write the equations of motion for a 3-body system in the x and y directions (see appendix A),

$$\ddot{x} = -GM \left(\frac{1}{r_1^2} \frac{x - X_1}{r_1} + \frac{1}{r_2^2} \frac{x - X_2}{r_2} \right), \quad (4)$$

$$\ddot{y} = -GM \left(\frac{1}{r_1^2} \frac{y - Y_1}{r_1} + \frac{1}{r_2^2} \frac{y - Y_2}{r_2} \right), \quad (5)$$

where G is the gravitational constant and M is the mass of each star (equal mass stars are assumed).

From Eq. (4) and (5) we can define:

$$v_x = \frac{dx}{dt}, \quad (6)$$

and

$$v_y = \frac{dy}{dt}, \quad (7)$$

for the x and y velocities of the planet respectively - forming two of the four first order equations required.

Subsequently, by a reformation of the two equations of motion in terms of the dimensionless variables t' , x' , y' , v'_x , v'_y , $r'_{1,2}$, $X'_{1,2}$, and $Y'_{1,2}$, we can derive the final two first order equations needed as the inputs for the Runge-Kutta algorithm. The replacements are as follows,

$$t' = \Omega t, \quad r'_{1,2} = \frac{r_{1,2}}{R}, \quad (8)$$

$$x' = \frac{x}{R}, \quad y' = \frac{y}{R}, \quad (9)$$

$$X'_{1,2} = \frac{X_{1,2}}{R}, \quad Y'_{1,2} = \frac{Y_{1,2}}{R}, \quad (10)$$

where v'_x and v'_y come from the implementation of these replacements in Eq. (4) and (5). After these substitutions and exploiting the connection between R and $\Omega - GM = R^3\Omega^2$ from Kepler's 3rd law, we arrive at,

$$\frac{dv'_x}{dt'} = \frac{1}{R\Omega^2} \frac{dv_x}{dt} = -\left(\frac{x' - X'_1}{r'^3_1} + \frac{x' - X'_2}{r'^3_2} \right), \quad (11)$$

and the equivalent in the y -direction,

$$\frac{dv'_y}{dt'} = \frac{1}{R\Omega^2} \frac{dv_y}{dt} = -\left(\frac{y' - Y'_1}{r'^3_1} + \frac{y' - Y'_2}{r'^3_2} \right). \quad (12)$$

Hence, we have found the four first-order differential equations which act as the input for the Runge-Kutta algorithm - Eq. (6), (7), (11) and (12).

2.2 Runge-Kutta Algorithm

The first-order equations listed in the previous section are input into the Runge-Kutta algorithm and four variables – x -position, y -position, x -velocity, and y -velocity are allowed to be changed manually in order to search for special types of orbit. When investigating certain orbit types, it is more useful to view them in the rotating frame of the stars. For example, if the planet moves in an ellipse around one star faster than the orbital period T , then in the fixed frame we would see a very complex motion opposed to simple

ellipses/circles in the rotating frame. The rotating frame is established through a change of variables when plotting the final function of the orbit, namely,

$$\begin{aligned}\xi &= x \cos \Omega t + y \sin \Omega t \\ \eta &= -x \sin \Omega t + y \cos \Omega t.\end{aligned}\tag{13}$$

This is computed and plotted alongside the fixed frame to investigate whether the orbit is stable or not. Orbits can be narrowed down by whether they return to a similar place in the rotating frame whilst precessing or if they form closed loops indicating they had completed an orbit and returned to their initial positions.

With this established, the next step is to enter the initial conditions for displacement and velocity and loop through the possibilities in order to search for interesting orbits. A function is defined that contains all of the initial conditions, including the length of time for which to run the program, τ , and finally calls the Runge-Kutta process. A suitable step size, N^{-1} , and value for τ are chosen which limits the error appropriately at each calculated variable whilst keeping the calculation time to a minimum. In order to determine this step size, the process is repeated for varying step sizes until the calculated orbit remained relatively constant regardless of changes in this parameter. Then, using this value for step size, a test is run with varying values of τ and a value is chosen which gave the full orbit with sufficient iterations to check stability but not too many iterations that time is wasted. For the most part, the value of τ chosen is 100,000 and a step size of 0.001. Using error analysis[4], the value for the fourth-order Runge-Kutta error is found to be 1.00×10^{-8} .

To investigate orbits around a single combined centre of mass or a single star (so-called ‘P-type’ orbits), the star-planet separation is made to be large. If sufficiently large, no matter what change in displacement along the x or y axis, a circular or elliptical orbit is returned. It is found that starting the planet on the x axis as opposed to on the y axis produces a change in the final orbit due to the stars being initially aligned on the x axis at positions $(0, R)$ and $(0, -R)$, where R is the radius of the circular path that they follow. Consequently, the breakdown of certain regimes of orbits is different for a planet initially starting from the x and y axes. Only planets starting at points along the axes are considered, as mapping out the orbits of the entire parameter-space would be too time-consuming and is outside of the scope of this paper. The input tangential velocity in the y direction and position in the x direction, or vice versa, are found from equating the forces active in circular motion,

$$F = \frac{GMm}{x^2} = \frac{mv_y^2}{x} \rightarrow v_y = \sqrt{\frac{2GM}{x}}.\tag{14}$$

This assumes a planet of negligible mass m , orbiting two stars, mass M , at distance x , as if they are one single body, where G is the gravitational constant and taking the tangential velocity of the circular motion at a point on the x axis where there is only velocity in the

y -direction. Under the change of variables to non-dimensionalise mentioned above, this becomes,

$$v_y = \sqrt{\frac{2}{x}}, \quad (15)$$

where M is the (combined) mass of the object that the planet is orbiting. This equation is used whilst decreasing the initial position, x (or y), to see where the boundary conditions lie for a circular orbit of the combined star system (see Section 3). The circular orbit of a single star whilst the other star acts as a small perturbation is also explored. In these cases, the planet must start within the radius of the orbiting stars such that the dominant gravitational force is from one of the stars not from the entire combined mass of the two stars. Cases in which the planet begins on either axis, and in either tangential direction are investigated and again, boundary conditions found. Chaotic orbits are discovered and are discussed in Section 3, but in most cases are not stable. Finally, other interesting stable orbits are found from varying choices of initial conditions, discussed fully in the next section. As an extension, habitable zones (zones where human life is possible) are discussed and plotted alongside the relevant orbits.

3 Results and Discussion

A number of interesting planetary orbits are discovered as a result of differing initial conditions. The purpose of this section is to document and explain the physics behind them. The most simple case is that of a circular orbit around both stars – a so-called P-type (planetary type) or circumbinary orbit. P type orbits occur when the planet is sufficiently far away from the binary system as to see the system like a single stationary mass located at the centre of mass of the two stars which happens to be the origin in our case. The planet is simply too far away to feel the difference in acceleration from star 1 and star 2 and orbits in a circle around the two. In actual fact, due to collisions with protoplanetary material or asteroids/comets, a circular orbit would be unlikely. Instead, protoplanets, which are planets forming out of the nebula from a star which has recently undergone a substantial mass loss, orbit in ellipses. However for the conditions assumed throughout this paper, a circular orbit is feasible. Both P type circular and elliptical orbits are explored, starting from a stable case at large radii, and decreasing the radii until the boundary condition for the breakdown of these types of orbits is found for planets starting from the x and y axes.

Another case of circular motion is that of the S-type (satellite type) orbit. Here, the planet orbits only one of the two stars with the other star acting as a perturbation. The boundary conditions for ejection of the planet from these sorts of orbits is examined. Which axis the planet initially starts from is crucial as the two stars are initially on the x axis within this model and so planets also starting from the x axis will start closer to

one star than the other. This allows the comparison of boundary conditions for planets beginning their motion from the x or y axis.

Non-circular S-type orbits are also investigated for initial displacements of 0 to $2R$. In these cases, the planet may orbit in an ellipse around one star and slowly precess, or it may complete one orbit a large distance from the primary star before completing a smaller one around the same star. The stability of such orbits are tested and the ranges in which these stable orbits can be found is discovered.

3.1 Circular P-type Orbits

For such orbits where the planet accelerates towards a single centre of mass at the origin following a circular path, simplified acceleration equations are needed. This system is analogous to Earth orbiting the Sun. The equations of motion are therefore,

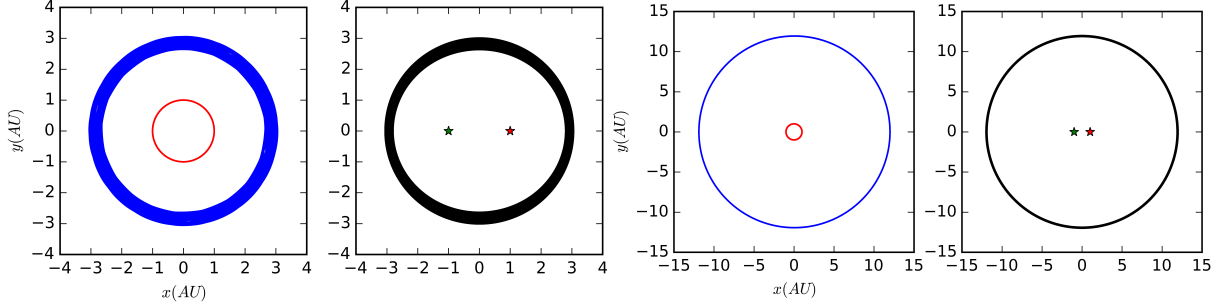
$$\ddot{x} = -\frac{2GM}{r^3}x, \quad (16)$$

$$\ddot{y} = -\frac{2GM}{r^3}y. \quad (17)$$

Using this, and Kepler's third law,

$$\frac{T^2}{4\pi^2} = \frac{r^3}{G(M_1 + M_2)} \quad (18)$$

we can arrive at the non-dimensionalised form which can be used computationally to search for such orbits. Using Eq. (15) to choose velocities, circular orbits are obtained as shown in Fig. 1 below for initial conditions starting on the x axis in the positive y direction.

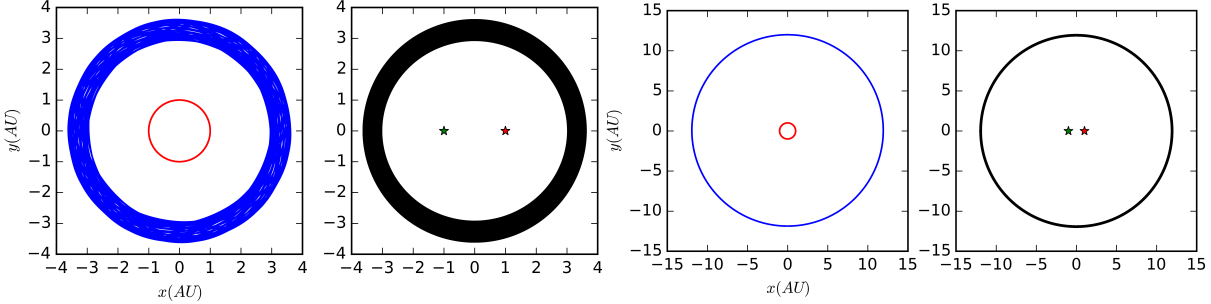


(a) An anticlockwise circular orbit at radius $2.8R$. (b) An anticlockwise circular orbit at radius $12R$.

Figure 1: LHS represents the fixed frame (blue lines for the orbit) and RHS represents the rotating frame (black lines for the orbit) with the two stars plotted for reference. Axes for both plots are identical and herein only one label will be shown to limit duplication. The red line represents the motion of the stars. For anticlockwise orbits starting on the x axis, (a) shows the boundary for stable circular P-type orbits at $2.8R$ and (b) a circular orbit at a large radius of $12R$.

A thicker line suggests that the orbit is not as stable because it is not returning to the exact same place. This can be seen in Fig. 1a which is on the boundary for stable circular orbits. Physically, this variation is caused by the gravitational attraction of the two stars becoming unequal as the planet approaches close enough to differentiate the stars as two separate bodies instead of one single body at the origin. Instead of being accelerated towards the origin, the planet feels the vector sum of the two gravitational forces from each star which perturbs the orbit, causing it to deviate from exactly circular and forming the thicker line observed. The boundary condition for a stable circular orbit is found to be x -position = $2.8R$, y -position = $0R$, x -velocity = $0R\Omega$, and y -velocity = $0.845R\Omega$.

The equivalent for a planet starting from the y axis can be seen in Fig. 2. As mentioned before, initially the stars are aligned on the y axis which leads to a difference in the boundary conditions for planets starting on one axis or the other.

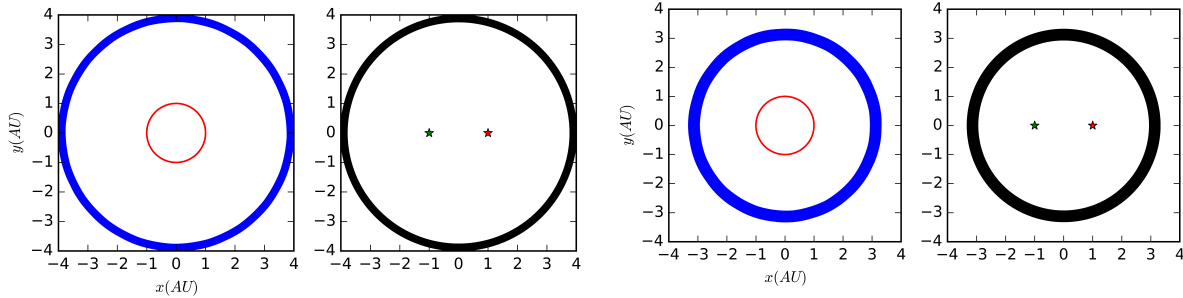


(a) An anticlockwise circular orbit at radius $3.6R$. (b) An anticlockwise circular orbit at radius $12R$.

Figure 2: For clockwise orbits starting on the y axis, (a) shows the boundary for stable circular P-type orbits at $3.6R$ and (b) a stable circular orbit at a large radius of $12R$.

For this case, the boundary conditions for a stable circular orbit are found to be x -position = $0R$, y -position = $3.6R$, x -velocity = $-0.745R\Omega$, and y -velocity = $0R\Omega$. Comparing Fig 1. and Fig 2. shows that at large enough radii, the orbit is independent on the axis the planet starts the simulation on. However, the boundary from circular orbit to an orbit where the planet is flung out of the system *does* depend on the starting axis. For planets starting the same distance away from both stars and with velocity so as to complete anticlockwise orbits (starting on the y axis), the boundary occurs at $3.6R$. Whereas for planets starting closer to one star and velocity so as to complete anticlockwise orbits (starting on the x axis), the boundary occurs closer in at $2.8R$.

The same can be done for planets starting with velocity in the opposite direction, that is, to complete clockwise orbits. As shown in Fig. 3 the boundaries for these cases are x -position = $4.0R$ and y -velocity = $0.707R\Omega$ (starting on the x axis) and x -position = $3.3R$ and y -velocity = $-0.778R\Omega$ starting on the y axis.



(a) A clockwise circular orbit at radius $4.0R$.

(b) A clockwise circular orbit at radius $3.3R$.

Figure 3: For clockwise orbits, (a) shows the boundary for stable circular P-type orbits starting on the x axis at $4.0R$ and (b) the same starting on the y axis at $3.3R$.

The condition for determining this boundary is to check how circular the orbit had become after 100 full orbits. If after this period of time the planet passes through the same position on each orbit with less than a deviation of 5 percent then it is considered circular. At this cut off, the orbit is plotted alongside the rotating frame and this is what is seen above when mentioning the boundaries.

As one can see, the orbits so far are almost identical apart from the radius that the boundaries occur - which is the key point that is being illustrated. For P-type orbits, as long as the planet resides within the boundary for circular motion, the orbits will remain uniform and not degrade over time. However, the variable that changes is where the boundary radius occurs for these different initial conditions.

3.2 Circular S-type Orbits

A slightly more interesting case is where the planet only orbits one of the two binary stars, with the other acting as a perturbation. For this to occur, the planet must be much closer to the star it orbits than to the other star in the system. Only small windows of stable orbits occur due to the increased proximity of stars leading to the increased probability of the ejection of the planet from the system. Orbit starting from both axes in both clockwise and anticlockwise directions are looked at. The most stable anticlockwise S-type orbit found is shown in Fig. 4.

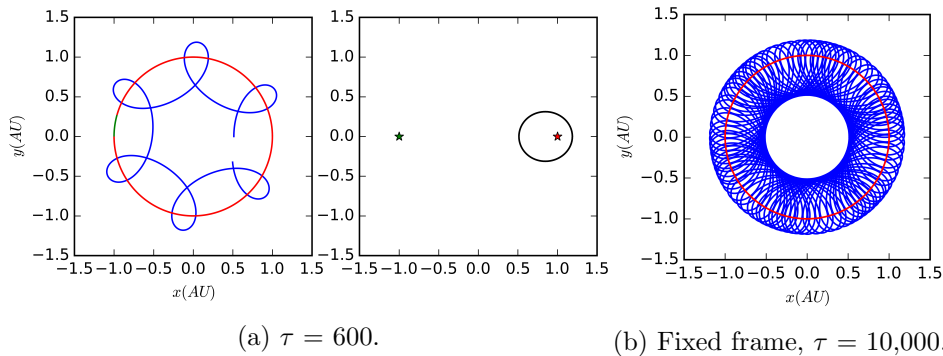


Figure 4: (a) Shows a stable S-type orbit displayed on a short time-scale of $\tau = 600$ so that it is possible to see the shape of the orbit. It occurs at $0.513R$ with initial conditions which should make it circular. However due to being close to the perturbing star, its orbit is stretched to an ellipse. (b) Shows the same but on a longer time-scale of $\tau = 10,000$, highlighting its stability over long periods of time.

This orbit roughly shows a 6:1 resonance, with the planet orbiting the primary star six times for every one period of the binary stars. It is not exact, causing the orbit to precess about the origin if viewed from the fixed frame. On long time-scales this causes

the orbit to appear as in Fig. 4a. One requirement of the stable S-type circular orbit is that the planet must orbit the primary star with a semi-major axis that does not pass too far over the midpoint between the two stars. This can be seen in Fig 4. by the fact that the closest the planet ever gets away from the primary star is $0.5R$. The perturbation of the secondary star is visible by the stretched out lobe effect of the orbit as the planet is pulled away from a circular orbit.

Similar S-type orbits to those mentioned above but with 5:1 and 3:1 resonances instead of 6:1 are shown in Fig. 5a and Fig. 5b below.

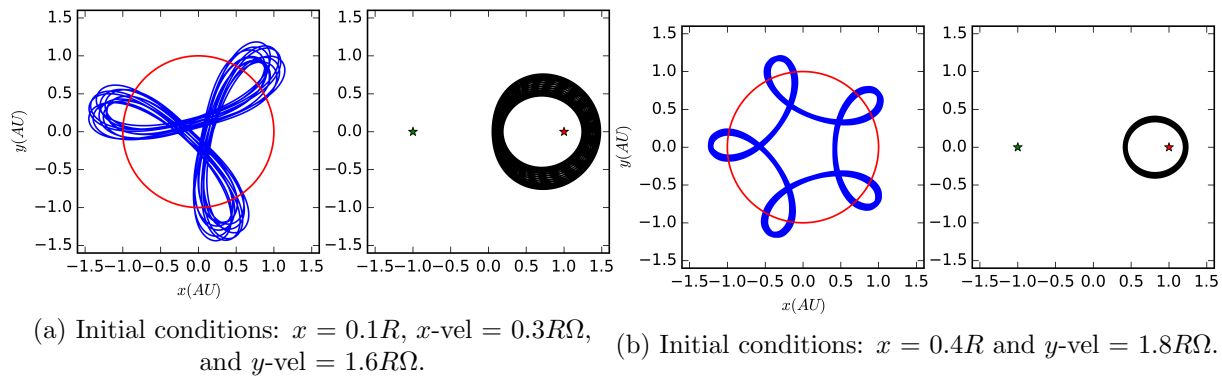


Figure 5: (a) Shows a less spatially stable 3:1 resonance whilst (b) shows a very spatially stable 5:1 resonance.

The 5:1 resonance found is less prone to precession over long periods of time when compared to the 6:1 or 3:1 resonance orbits found, as visible from the spread of the orbit.

3.3 Boundary Conditions

The boundary is difficult to define for orbits. As one approaches the boundary, orbits may look stable but when looking at the next orbit on, it is clearly not as the planet has been ejected. The next orbit on might even be stable again and so on until it becomes fully stable. This shows that near boundaries chaos plays a role – with a very small change in variables producing a completely different result. Whilst some orbits are merely ejected, others are flung out to stable orbits at much greater radii from which they started.

The boundary conditions of the orbits mentioned in Fig. 4 are investigated and the radii at which these S-type orbits break down found to be $0.449R$ and $0.589R$ as shown in Fig. 6 below.

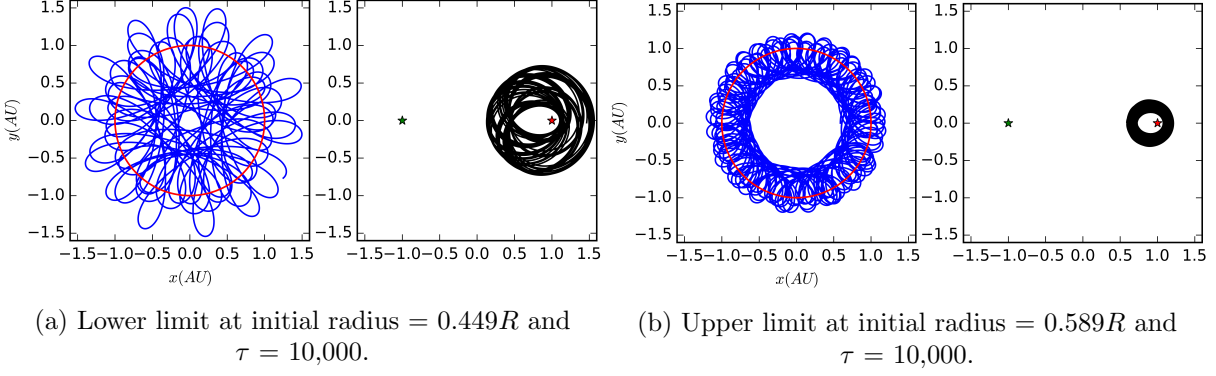


Figure 6: (a) Shows the lower boundary for a stable circular S-type orbit, due to the planet getting too close to the secondary star. (b) Shows the upper boundary for the same type of orbit, due to the planet getting too close to the primary star.

Near the lower end of the boundary the orbit is erratic and bordering on chaotic, a topic discussed in more detail in Section 3.5. The planet approaches the mid-point between the two stars, such that if it went any further the secondary star would create a bigger gravitational force than the first, cease to be the perturbing star and pull it out of its orbit. On the other end of the spectrum, when the planet starts closer to the primary star, it follows an S-type orbit with much smaller radius, and hence has a larger velocity and orbits many more times per binary period than in the former case, as shown by the increased density of lines in Fig. 6b compared to Fig. 6a.

These boundary conditions are pushed until breaking point, with the resulting behaviour outlined in Fig. 7.

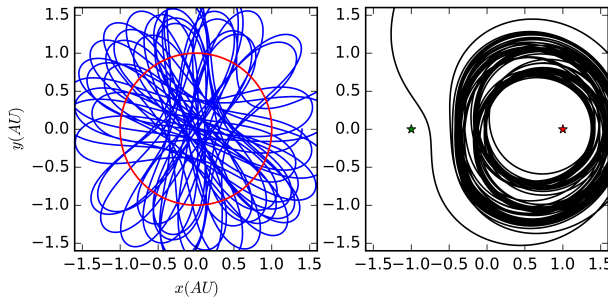


Figure 7: Figure shows what happens when pushing the boundaries to breaking point. The clockwise S-type orbit gets too close to the secondary star which pulls it out of its orbit and ejects the planet from the system.

The effects of the perturbation becoming dominant are clearly visible and highlight how unstable an orbit can be near the boundary. Another example of an orbit near a boundary is where the orbit is nearly stable but gets too close to one of the stars and is ejected

from the system. This is illustrated in Fig. 8, for initial conditions of x -position = $0R$, y -position = $3.34R$, x -velocity = $-0.774R\Omega$, and y -velocity = $0R\Omega$ similar to in Fig. 2.

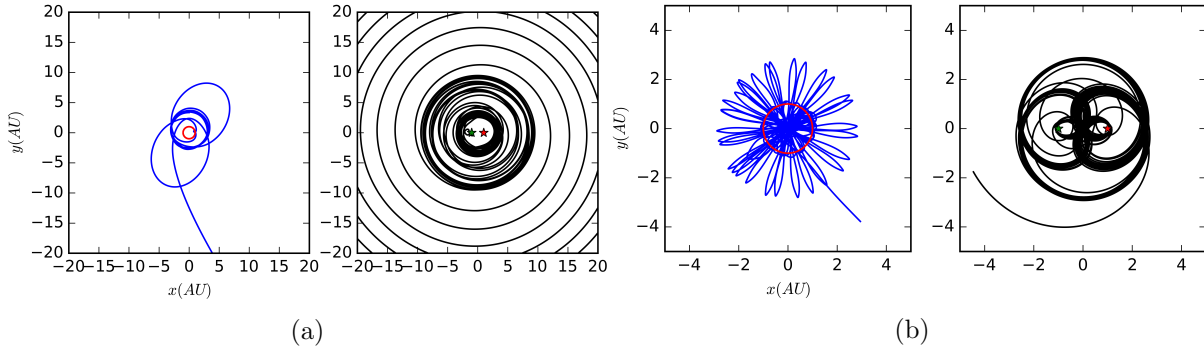


Figure 8: (a) and (b) show a near-stable orbit close to the boundary conditions being ejected from the system.

On small time scales such orbits may seem stable, but when run for longer periods of time it is clear that this is not the case.

3.4 Non-Circular Orbits

When the initial velocity is not determined through Eq. (15) and can take any value, we observe non-circular S-type orbits. The only non-circular P-type orbits are ellipses and as stated previously, the emphasis of this paper is to focus on the circular forms of the P-type orbits. However, it is worth stating that in these cases one would observe an elliptical orbit similar to the orbits of the planets in our solar system or an ellipse that precesses such that its apogee traces a circular path instead of remaining constant in space. A number of different P-type orbits with symmetries are observed, however many precessed around the origin. These are displayed in Fig. 9.

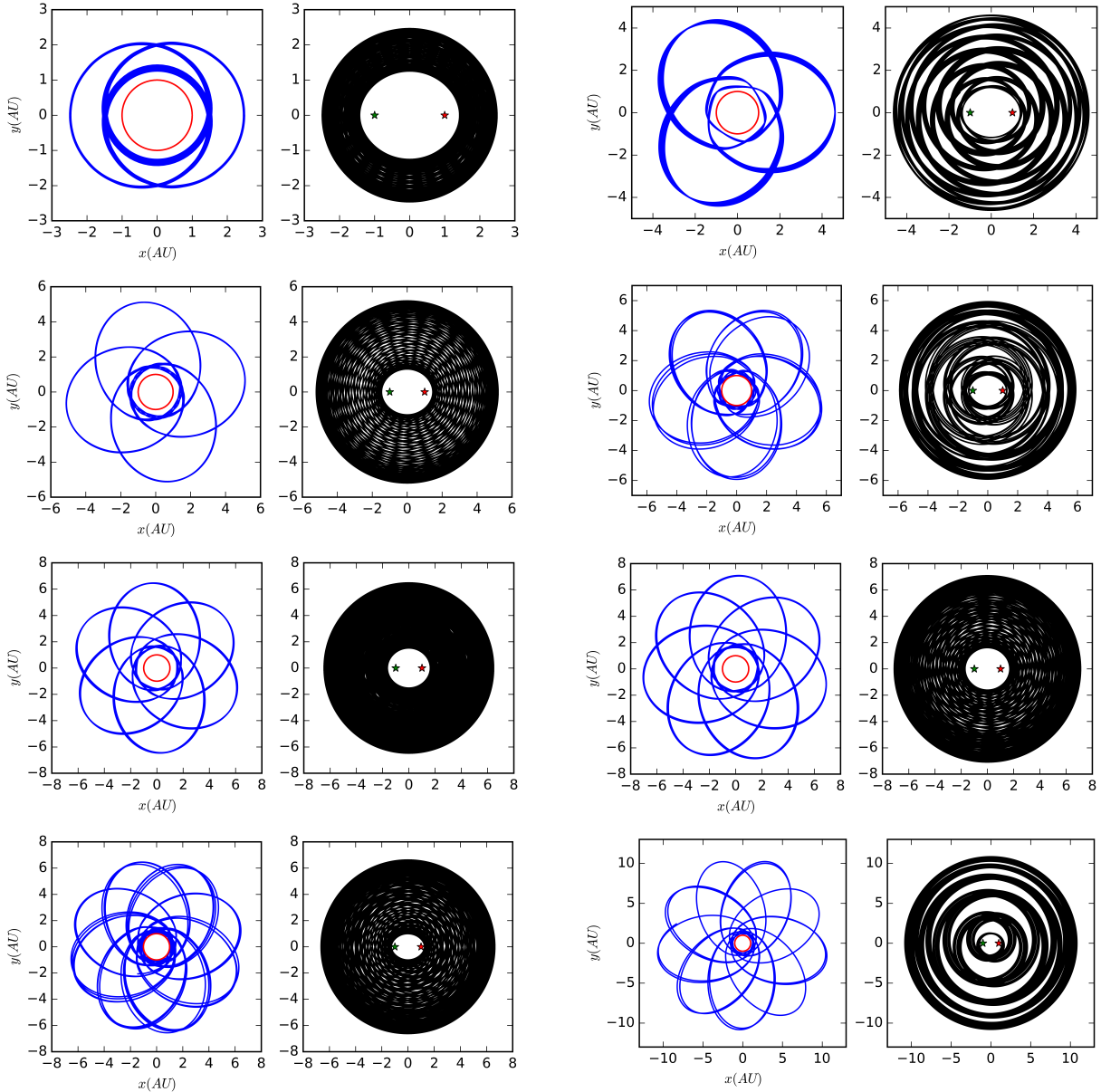


Figure 9: Following the figures in reading order, they show P-type orbits with 2 to 8-fold symmetries respectively with the symmetry increasing by one per each image.

These symmetries continue indefinitely and Fig. 9 is meant to illustrate the plethora of orbital solutions available. They are created by simulating random values of x -displacement, y -displacement, x -velocity, and y -velocity from 0 to 2 in intervals of 0.1. Whilst keeping x or y -displacement constant, the other three variables are changed which resulted in many solutions to search through. As this project is computationally limited, searching only along the axes is quicker than changing all four variables at once. The long term stability

is tested and all but the 5-fold, 7-fold, and 8-fold solutions are found to not substantially precess over a period of 100,000 orbits. The 2-fold symmetrical orbit changes its radial separation as it repeatedly travels closer to the stars completing half an orbit, then further away completing nearly a full elliptical orbit then travels back in again.

In addition to these, other P-type orbits are found that exhibit interesting traits. One class of orbit is an S-type whose radius extends further than the midpoint between the two stars. Although appearing normal in the rotating frame, this class trace interesting paths which do not overlap until returning approximately to the start position. This is illustrated below in Fig. 10.

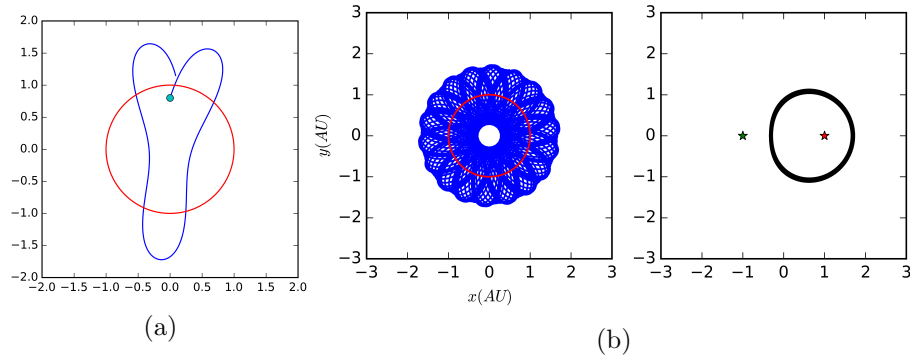


Figure 10: (a) Shows the shape of this particular class of orbit with a blue marker on the initial position of the planet.(b) Shows a longer time period elapsed.

Finally, there are some orbits discovered which are S-type but with a slight difference to those mentioned before. These types of orbit are elongated *away* from the secondary star. This suggests that they have enough velocity to overcome the affects of the perturbation and begun as an elliptical orbit with perihelion on the side closest to the perturbing star. Fig. 11 illustrates this effect.

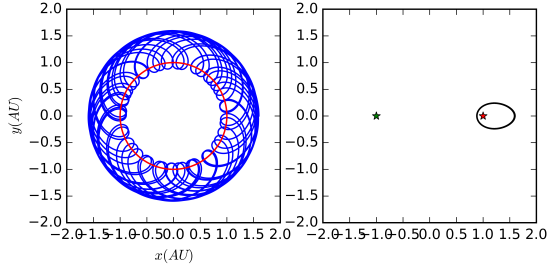


Figure 11: Figure shows an elliptical S-type orbit with its perihelion on the side closest to the perturbing star.

It is possible that many other exotic orbits exist but due to the lack of computational power they are outside of the scope of this paper.

3.5 Chaotic Orbits

Chaotic orbits have the tendency to change their orbital period with no repetition and as such, often get ejected from the binary system. An orbit can be classified as chaotic when the gravitational effects from the binary star sum in unpredictable ways such that the orbital path is considered random[5]. Resonance, the effect celestial bodies aligning to produce an enhanced gravitational pull, can cause some orbits to become chaotic. For example, in a true binary system model, many planets may orbit in such a way to create resonances and eventually one planet may be pulled from its stable orbit into a chaotic one which will in most cases lead to the ejection of the planet. This normally happens on long time-scales, much longer than a human lifespan[6]. Chaotic orbits are sensitive to very small changes in initial conditions which is why the boundary orbits mentioned in previous sections could be described as such. Fig. 12 below shows an example of chaotic orbits found via the Runge-Kutta simulation.

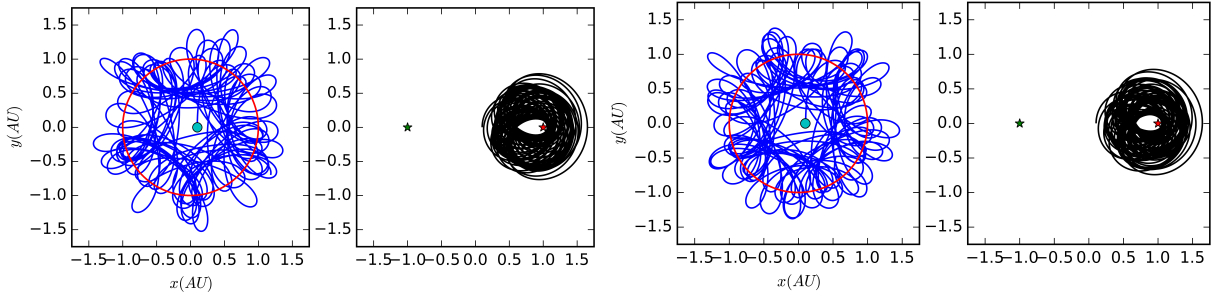


Figure 12: Both (a) and (b) are examples of chaotic S-type orbits. This is shown by changing the initial x -position by only $0.005R$ and observing a completely different orbital path.

Clearly, these types of orbits do not follow a predictable path because only small changes in initial conditions completely offset the previous orbit. Such orbits would never be considered habitable for human life due to the extreme changes in distance from the stars.

3.6 Habitable Zones

In order to investigate the habitability of the P-type orbits discovered, a method taking the input parameters and calculating a specific habitable zone (HZ) of a binary system was used[7]. It was chosen to constrain the habitability using a general habitable zone (GHZ), which have lower limits bordered by the runaway greenhouse effect and upper limits bordered by the maximum greenhouse effect[8]. The masses of the binary companions are considered to be $1M_{\odot}$, with luminosity $1L_{\odot}$, temperature 3000K, and separated by 1AU, whilst the mass of the planet is set to $1M_{\oplus}$. Under these constraints, a GHZ was calculated and plotted over the orbits discovered. The HZ ranges from 2.39AU to 3.11AU and it is found that only the orbit displayed in Fig. 1 fell within this zone.

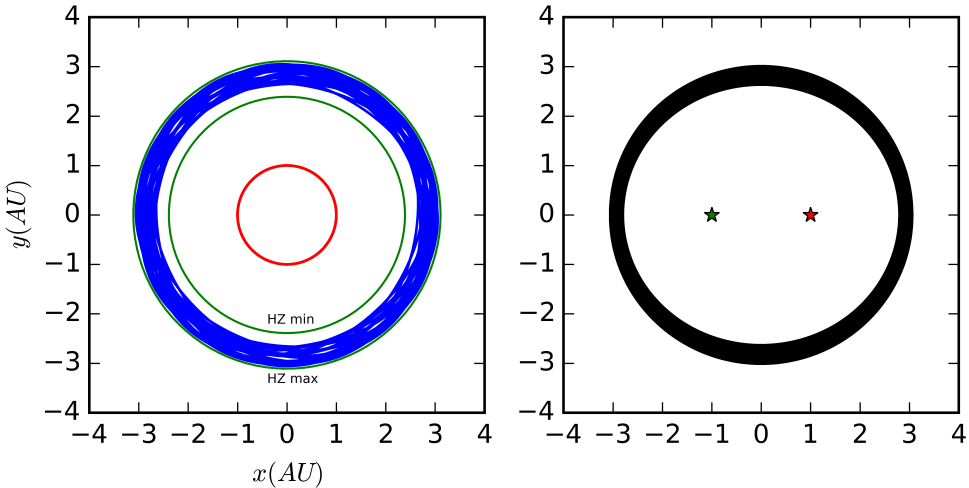


Figure 13: A P-type orbit at $2.8R$ is found to fall within the habitable zone. The green lines mark the HZ boundaries at 2.39AU to 3.11AU.

It is worth noting that this particular orbit stayed within the GHZ between the temperature range 3000 – 4000K for the binary stars placing them as category M or K, whereas our sun is a category G star at 5772K[9]. All other orbits found did pass through the GHZ but not remain within it, suggesting that they would not be considered habitable. Under more lenient definitions of habitable zones, for example the extended habitable zone, other orbits discovered may be classed as habitable.

3.7 Additional Research and Limitations

There are a few further extensions of this work worth mentioning. Firstly, the assumption that a binary system will be exactly separated by 1AU with both stars of exactly equal mass is not a good one. In most cases of a binary system, one star is more massive than the other and sometimes even is close enough to accrete matter from the other star. Considering a scenario where one star accretes matter from the other, then as the star's mass is now a function of time, so will the gravitational field produced by it. A changing gravitational field would alter the path of a planet substantially over enough time. This is an example of one area of study worth investigating.

A model that incorporates the effects of the planet's course being altered by an external variable would be interesting to explore. In some systems asteroids and comets will be present which, on collision, can drastically alter the orbit of a planet. Some strong stellar winds are also known to alter the path of small projectiles.

It is unlikely that only one planet will be present in any solar system. The addition of multiple planets would lead to resonance effects, which could alter stable orbits and turn them into chaotic ones or perhaps vice versa. If considered at a protoplanetary stage in evolution, the formation of planets and their satellites could be modelled. Such a model would be a more realistic playground to test habitability and aid our search for exoplanets.

Liberator-type (L-type) orbits, in which the planet is located at the Lagrangian L_4 and L_5 points have not been considered. It is suggested that these are only stable for cases where the mass ratio of the binary stars is smaller than 0.04[3]. Although it is unlikely that any planet would be captured at this point, if formed at this position it leads to the possibility of additional stable planetary orbits.

This project is mainly limited by its simplicity. For example, a solar system is assumed where there is only a binary system and planet surrounded by a vacuum. In reality, dust particles would be present in replacement of the vacuum and they may form asteroids and comets that would affect the path of any orbit. This assumption, along with the lack of additional areas of research included in the model, make for a simulation that is too basic to compare to the real binary systems we observe.

4 Conclusion

Using the Runge-Kutta algorithm, many orbital scenarios for a planet in a binary star system are explored. The vast majority of the orbits produced are so-called P-type, meaning that the star orbits both stars as if they are one. Many circular forms of this type of orbit are found, and the boundary conditions for these tested. It is found that for anticlockwise orbits starting on the x axis, the boundary is $2.8R$ whereas when starting on the y axis, equal distance from both stars, the boundary is $3.6R$. For clockwise orbits, planets initially on the x axis reached a boundary for circular orbits at $4.0R$ compared to $3.3R$ for the same starting on the y axis. The same is investigated for orbits where the planet only circled one of the two stars (S-type orbits). These S-type orbits are found to reside within a range of $0.449R$ and $0.589R$ with $0.513R$ being the most stable.

The point where boundary conditions break is looked at, and it is concluded that orbits become more chaotic as this region is approached due to the planet's increased proximity to the stars. As the planet approaches the stars, they pull it from a stable orbit and it is often ejected. Some cases are found where a seemingly stable orbit suddenly ceases as the planet is ejected from the system. A range of non-circular orbits are examined, with 2 to 8-fold symmetries shown and long term stability tested. As an extension, chaotic orbits are discussed, and an example presented showing the slight change in initial conditions producing a completely different orbital path. Habitable zones are covered, and simulated for our binary star example by comparison to Alpha Centauri, a similar system. A huge range of planetary orbits are available when all position and velocity variables are allowed to change on small scales, with only a small but representative subsection presented in this paper.

Appendix A: Equations of Motion for a 3-Body System

The required equations to search for stable orbits are Eq. (4) and (5). In order to arrive at these, the planet's gravitational attraction to the two stars and Newton's laws must be combined. The purpose of this appendix is to show this derivation.

Consider the gravitational force felt by a planet of negligible radius and mass, m , due to two stars (1 and 2) of equal mass M , a distance R from the origin, and at a distance r_1 and r_2 respectively from the planet.

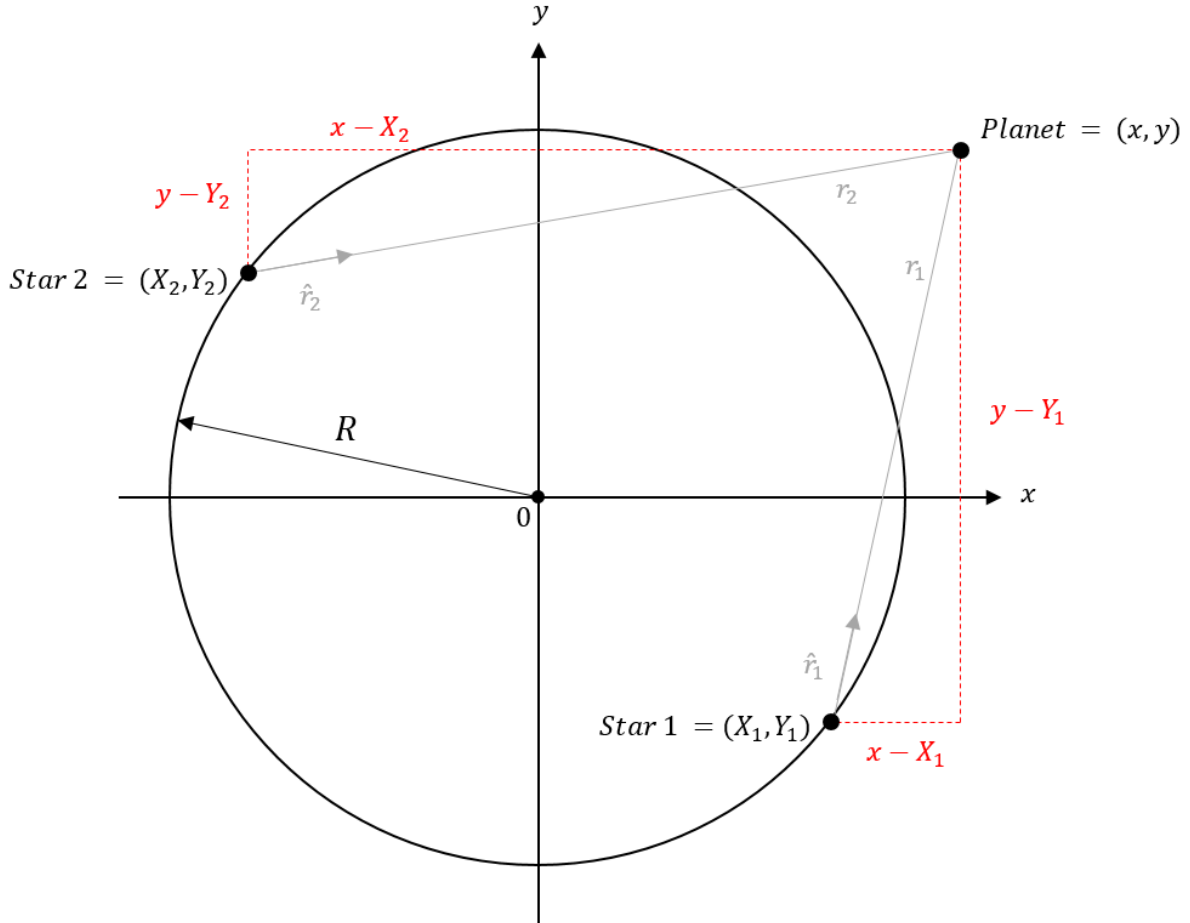


Figure 14: Diagram showing all distances involved in the 3-body system of a planet and two binary stars.

This is shown above in Fig. 14 and we find this gravitational force has the functional

form,

$$\mathbf{F} = -\frac{GMm}{r_1^2}\hat{\mathbf{r}}_1 - \frac{GMm}{r_2^2}\hat{\mathbf{r}}_2 = m\mathbf{a}, \quad (19)$$

where G is the gravitational constant, $\hat{\mathbf{r}}_1$ and $\hat{\mathbf{r}}_2$ are unit vectors in the direction of a straight line between the planet and star 1 and 2 respectively, and \mathbf{a} is the acceleration of the planet. Newton II has been used to equate this gravitational force to the motion of the body via $\mathbf{F} = m\mathbf{a}$. Writing the unit vectors in terms of x and y -components we have,

$$\hat{\mathbf{r}}_1 = \frac{x - R \cos(\Omega t)}{r_1} \hat{\mathbf{x}} + \frac{y - R \sin(\Omega t)}{r_1} \hat{\mathbf{y}}, \quad (20)$$

$$\hat{\mathbf{r}}_2 = \frac{x + R \cos(\Omega t)}{r_2} \hat{\mathbf{x}} + \frac{y + R \sin(\Omega t)}{r_2} \hat{\mathbf{y}}. \quad (21)$$

With these replacements,

$$\begin{aligned} \mathbf{a} = & -GM \left(\frac{x - R \cos(\Omega t)}{r_1^2} + \frac{x + R \cos(\Omega t)}{r_2^2} \right) \hat{\mathbf{x}} \\ & -GM \left(\frac{y - R \sin(\Omega t)}{r_1^2} + \frac{y + R \sin(\Omega t)}{r_2^2} \right) \hat{\mathbf{y}}. \end{aligned} \quad (22)$$

Decomposing this into x and y components, and defining the following variables,

$$\begin{aligned} X_1 &= R \cos(\Omega t), & Y_1 &= R \sin(\Omega t), \\ X_2 &= -R \cos(\Omega t), & Y_2 &= -R \sin(\Omega t), \end{aligned}$$

yields two equations for the acceleration in the x and y directions,

$$\ddot{x} = -GM \left(\frac{1}{r_1^2} \frac{x - X_1}{r_1} + \frac{1}{r_2^2} \frac{x - X_2}{r_2} \right), \quad (23)$$

$$\ddot{y} = -GM \left(\frac{1}{r_1^2} \frac{y - Y_1}{r_1} + \frac{1}{r_2^2} \frac{y - Y_2}{r_2} \right). \quad (24)$$

These are the two equations of motion which we begin from in Section 2.

References

- [1] Aguilar, D. (2013). Most Milky Way Stars Are Single. [online] www.cfa.harvard.edu/. Available at: <https://www.cfa.harvard.edu/news/2006-11> [Accessed 4 May 2016].
- [2] Roberts Jr., L., Tokovinin, A., Mason, B., Riddle, R., Hartkopf, W., Law, N. and Baranec, C. (2015). Know the Star, Know the Planet. III. Discovery of Late-Type Companions to Two Exoplanet Host Stars. *The Astronomical Journal*, 149(4), p.118.
- [3] Dvorak, R. (1986). Critical Orbits in the Elliptic Restricted Three-Body Problem. *Astron. and Astrophysics*, 167, pp.379-386.
- [4] Fitzpatrick, R. (29/03/2006). Runge-Kutta methods. [online] Farside.ph.utexas.edu. Available at: <http://farside.ph.utexas.edu/teaching/329/lectures/node35.html> [Accessed 3 May 2016].
- [5] Laskar, J. (1996). Large scale chaos and marginal stability in the solar system. *Celestial Mechanics and Dynamics Astronomy*, 64(1-2), pp.115-162.
- [6] Hayes, W. (2007). Is the outer Solar System chaotic?. *Nat Phys*, 3(10), pp.689-691.
- [7] Cuntz, M., Bruntz, R. (2013). A Numerical Tool for the Calculation of S/P-Type Habitable Zones in Binary Systems.
- [8] Cuntz, M. (2013). S-Type and P-type Habitability in Stellar Binary Systems: A Comprehensive Approach. I. Method and Applications. *ApJ*, 780(1), p.14.
- [9] Williams, D. (2016). Sun Fact Sheet. [online] Nssdc.gsfc.nasa.gov. Available at: <http://nssdc.gsfc.nasa.gov/planetary/factsheet/sunfact.html> [Accessed 3 May 2016].